








CDK7 and MITF repress a transcription program involved in survival and drug tolerance in melanoma

Pietro Berico^{1,2,3,4} , Max Cigrang^{1,2,3,4} , Guillaume Davidson^{1,2,3,4}, Cathy Braun^{1,2,3,4}, Jeremy Sandoz^{1,2,3,4}, Stephanie Legras^{1,2,3,4}, Bujamin Hektor Vokshi^{1,2,3,4} , Nevena Slovic^{1,2,3,4} , François Peyresaubes^{1,2,3,4}, Carlos Mario Gene Robles^{1,2,3,4}, Jean-Marc Egly^{1,2,3,4} , Emmanuel Compe^{1,2,3,4}, Irwin Davidson^{1,2,3,4,*}  & Frederic Coin^{1,2,3,4,**} 

Abstract

Melanoma cell phenotype switching between differentiated melanocytic and undifferentiated mesenchymal-like states drives metastasis and drug resistance. CDK7 is the serine/threonine kinase of the basal transcription factor TFIIF. We show that dedifferentiation of melanocytic-type melanoma cells into mesenchymal-like cells and acquisition of tolerance to targeted therapies is achieved through chronic inhibition of CDK7. In addition to emergence of a mesenchymal-type signature, we identify a GATA6-dependent gene expression program comprising genes such as *AMIGO2* or *ABCG2* involved in melanoma survival or targeted drug tolerance, respectively. Mechanistically, we show that CDK7 drives expression of the melanocyte lineage transcription factor MITF that in turn binds to an intronic region of GATA6 to repress its expression in melanocytic-type cells. We show that GATA6 expression is activated in MITF-low melanoma cells of patient-derived xenografts. Taken together, our data show how the poorly characterized repressive function of MITF in melanoma participates in a molecular cascade regulating activation of a transcriptional program involved in survival and drug resistance in melanoma.

Keywords CDK7; TFIIF; MITF; melanoma; GATA6

Subject Categories Cancer; Chromatin, Transcription & Genomics; Signal Transduction

DOI 10.15252/embr.202051683 | Received 7 September 2020 | Revised 18 June 2021 | Accepted 25 June 2021 | Published online 23 July 2021

EMBO Reports (2021) 22: e51683

Introduction

Malignant melanoma is responsible for 70% of skin cancer deaths in Western countries (Eggermont *et al*, 2014). Somatic gain-of-function mutations in the proto-oncogene kinase *BRAF* are the commonest mutations (60%) with the T → A transversion underlying *BRAF*^{V600E} comprising the majority of *BRAF* mutations (Brose *et al*, 2002; Davies *et al*, 2002). As an alternative to *BRAF* mutations, human melanomas frequently (35%) carry *NRAS* or *NF1* mutations, while the remainder (5%) shows no mutations of these three genes (Triple-Wt) (Hodis *et al*, 2012).

Melanoma is notorious for its heterogeneity based on co-existing melanoma cell phenotypes. *In vitro*, transcriptomic analysis of melanoma cells has established two main and distinct signatures defined as either melanocytic-type (proliferative) or mesenchymal-like (invasive) melanoma cell states (Carreira *et al*, 2006; Widmer *et al*, 2012; Verfaillie *et al*, 2015). At the transcriptional level, the differentiated melanocytic-type melanoma cells display high levels of lineage-specific transcription factors, including the *SRY-box 10* (*SOX10*) and the *Microphthalmia-associated Transcription Factor* (*MITF*) that drive expression of melanocyte lineage genes. Undifferentiated mesenchymal-like melanoma cells express low levels of *MITF* and *SOX10*, and their gene expression signature, including markers like the *AXL receptor tyrosine kinase* (*AXL*) and *SOX9*, is driven by AP1-TEAD factors (Verfaillie *et al*, 2015; Minnoye *et al*, 2020). The discovery of cells with intermediate signatures (Ennen *et al*, 2017; Wouters *et al*, 2020) supports the initial concept of phenotypic plasticity driving melanoma progression through conversion from one phenotype into another in response to external cues (Hoek *et al*, 2008; Ennen *et al*, 2017; Rambow *et al*, 2018).

Treatment options for patients with metastatic melanoma include combination therapies with inhibitors targeting the *BRAF* (i.e.,

1 Institut de Génétique et de Biologie Moléculaire et Cellulaire, Equipe Labélisée Ligue contre le Cancer, Strasbourg, France

2 Centre National de la Recherche Scientifique, UMR7104, Illkirch, France

3 Institut National de la Santé et de la Recherche Médicale, Illkirch, France

4 Université de Strasbourg, Illkirch, France

*Corresponding author. Tel: +33 3 88653445; E-mail: irwin@igbmc.fr

**Corresponding author. Tel: +33 3 88653270; E-mails: fredr@igbmc.fr

vemurafenib and dabrafenib) and MEK (i.e., trametinib) kinases (BRAFi and MEKi, respectively), whose efficiency is limited by development of resistance and subsequent progression (Menzies & Long, 2014). It is well established that tolerance to targeted therapies can involve various phenotype changes, including epithelial–mesenchymal transition(-like) (EMT) from a melanocytic to a mesenchymal state (Kemper *et al*, 2014; Arozarena & Wellbrock, 2019; Rambow *et al*, 2019). Therefore, understanding the molecular details of phenotypic plasticity and transcriptional reprogramming of melanoma cells is crucial for the development of future therapeutic approaches.

Among the protein complexes essential for gene expression in eukaryotes, the basal transcription factor TFIID is unique due to its various enzymatic activities, including helicase, translocase, and kinase functions (Villicana *et al*, 2014; Berico & Coin, 2018). The CDK7 subunit of TFIID is a kinase that phosphorylates transcription factors, including the largest subunit of RNA polymerase II, to promote gene expression (Eick & Geyer, 2013; Compe & Egly, 2016; Fisher, 2019). Surprisingly, CDK7 kinase activity inhibition (CDK7i) elicits dramatic responses in various cancers (Cao & Shilatifard, 2014; Christensen *et al*, 2014; Kwiatkowski *et al*, 2014) probably due to the contribution of the TFIID kinase in super-enhancer (SE)-linked oncogene transcription (Chipumuro *et al*, 2014). SEs are broad genomic regions that drive transcription of cell identity genes in normal tissue or oncogenes in cancer (Hnisz *et al*, 2013). SEs are enriched in specific transcription factors such as CDK7, Mediator, the BET family of bromodomain protein 4 (BRD4), or chromatin marks such as H3K27 acetylation (H3K27ac) (Whyte *et al*, 2013). Besides CDK7i, inhibition of BRD4 (BETi) with the small molecule JQ1 causes loss of expression for many SE-associated genes in cancer cells (Loven *et al*, 2013).

Here, we show that resistance to CDK7i correlated with melanoma cell dedifferentiation and acquisition of tolerance to BRAF and MEK inhibitors. Besides the mesenchymal-like signature, we observed the emergence of a transcription program comprising genes involved in melanoma survival and drug tolerance under the control of the *GATA-binding factor 6 transcription factor* (GATA6). CDK7 prevents the emergence of the GATA6-dependent transcription program in differentiated melanoma cells by promoting the SE-dependent expression of MITF that binds to an intronic regulatory sequence of the GATA6 locus to silence its expression. In agreement with findings in cell cultures, we observed that diminished MITF expression during human melanoma progression and phenotype switching promotes the progressive activation of GATA6 in patient-derived xenografts. We determined that GATA6 emerges in the MITF-low cells of the PDX showing invasive or interferon γ (IFN γ)-active phenotypes.

Results

Melanoma cultures exhibit distinct sensitivity to CDK7i

We explored the sensitivity of melanoma cells to CDK7i using cells with the two main phenotypes and most common driver mutations. The melanocytic-type patient-derived MM011 (NRAS^{Q61K}), MM074 (BRAF^{V600E}), MM117 (Triple-wt) cell cultures and the melanoma 501mel cell line (BRAF^{V600E}) exhibited moderate to high expression

of the lineage-specific transcription factors MITF and SOX10 together with low to undetectable levels of SOX9 and c-JUN (Widmer *et al*, 2012; Verfaillie *et al*, 2015) (Fig 1A). In contrast, patient-derived MM029 (BRAF^{V600K}), MM047 (NRAS^{Q61R}), and MM099 (BRAF^{V600E}) cell cultures showed a mesenchymal-like phenotype characterized by low to undetectable levels of MITF and SOX10 coupled to high levels of SOX9 and c-JUN (Widmer *et al*, 2012; Verfaillie *et al*, 2015; Wouters *et al*, 2020). We observed that all melanocytic-type cells together with the MM047 mesenchymal-like cells were sensitive to low concentrations of THZ1, the first-in-class selective and covalent inhibitor of CDK7 (Kwiatkowski *et al*, 2014) (Fig 1B). In marked contrast, the MM099 and MM029

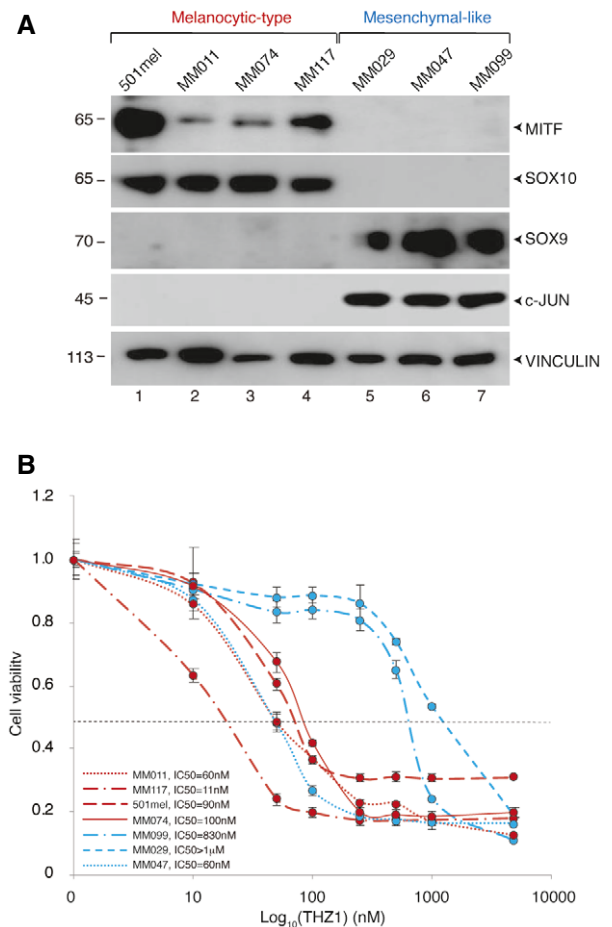


Figure 1. Melanoma cells show differential sensitivity to CDK7i.

A Protein lysates from the melanocytic-like melanoma cells 501mel, MM011, MM074, and MM117 or the mesenchymal-like melanoma cells MM029, MM047, and MM099 were immuno-blotted for proteins as indicated. Molecular mass of the proteins is indicated (kDa).

B Melanoma cells were treated with increasing concentrations of THZ1 as indicated for 72 h. Mean growth is shown relative to vehicle (DMSO)-treated cells. IC50 for each cell line is indicated. Melanocytic-type (MITF-High, proliferative) melanoma cells are shown in red, while mesenchymal-like (MITF-low, invasive) melanoma cells are shown in blue.

Data information: In (B), data are presented as mean values + standard deviation (SD) for three replicates ($n = 3$). Source data are available online for this figure.

mesenchymal-like cells were tolerant to CDK7i, even at high concentrations of the drug. These observations demonstrated that melanocytic-type melanoma cells were highly sensitive to CDK7i, regardless of their driver mutation, while some mesenchymal-like melanoma cells were tolerant to the drug.

CDK7i promotes dedifferentiation of melanoma cells

To investigate the role of CDK7 in melanoma cells, we generated several THZ1-resistant (CDK7i) or vemurafenib-resistant (BRAFi) cell lines *ex vivo* (MM074^{CDK7i-R}, MM074^{BRAFi-R}, and MM047^{CDK7i-R}) (Fig EV1A–C). Establishment of CDK7i resistance decreased sensitivity of the MM074^{CDK7i-R} to BRAFi (vemurafenib) and MEKi (trametinib) (Fig EV1B and D), while the BRAFi-resistant MM074^{BRAFi-R} remained sensitive to both CDK7i and MEKi (Fig EV1A and D). In agreement with the involvement of CDK7 in gene expression, global transcription activity of MM047 and MM074 was strongly impacted by CDK7i treatment, in contrast to MM047^{CDK7i-R} and MM074^{CDK7i-R} where global transcription was not inhibited (Fig EV1E).

RNA-seq revealed a pronounced modification of the transcriptional programs of MM074^{CDK7i-R} and MM074^{BRAFi-R} compared to the parental MM074, but a less pronounced modification of the MM047^{CDK7i-R} compared to MM047 (Fig 2A). More than 6,000 genes were deregulated in MM074^{CDK7i-R} compared to MM074 and 1,000 genes in MM047^{CDK7i-R} compared to MM047 (Fig 2B). Despite the fact that the parental cells were of different phenotypes, 261 genes were commonly up-regulated in the two CDK7i-resistant cell cultures (Fig 2B and Dataset EV1). We hereafter defined these genes as the “CDK7i-resistant signature” (K7iRS). As shown by Gene Ontology (GO) analysis, these genes were involved in epithelial cell differentiation or in the transport of small molecules (Appendix Fig S1).

We next clustered melanoma cells based on the expression of a hundred genes corresponding to previously described signatures of melanocytic *vs* mesenchymal transcriptional cell states (Widmer *et al*, 2012). In agreement with the literature (Verfaillie *et al*, 2015; Wouters *et al*, 2020), 501mel and MM074 showed a melanocytic-type transcriptional signature (Fig 2C, lanes 1–2), while the MM047, MM099, and MM029 cells showed a mesenchymal-like signature (lanes 5–7). Surprisingly, chronic exposure of MM074 to CDK7i induced the emergence of a stable mesenchymal-like signature (compare lane 2 with 4) correlating with increased invasion capacity

(Fig EV1F). In apparent contrast with MM074^{CDK7i-R}, the melanocytic-type signature of MM074 persisted in MM074^{BRAFi-R} where we further observed a significant increase in the expression of a set of *bone fide* pigmentation genes (Fig 2C, compare lane 2 with 3). RT–qPCR confirmed the increased expression of genes involved in pigmentation such as *MLANA* in MM074^{BRAFi-R} (Fig EV1G), which correlated with higher cellular pigmentation (Fig EV1H). In agreement with mRNA, we observed that the MM074^{BRAFi-R} exhibited significantly higher amounts of the melanocyte lineage-specific proteins MITF and TFAP2A compared to MM074 (Fig 2D, compare lane 1 with 2). In contrast, MM074^{CDK7i-R} showed a dramatic decrease of these proteins together with the emergence of SOX9 (compare lane 1 with 3).

Altogether, these data showed that MM074 melanocytic-type cells chronically exposed to CDK7i dedifferentiated to adopt a mesenchymal state, whereas those exposed to BRAFi acquired a highly pigmented hyper-differentiated cell state. Furthermore, both mesenchymal-like and melanocytic-type melanoma cells chronically exposed to CDK7i displayed common altered expression of 261 genes corresponding to the K7iRS.

A GATA6-dependent transcription program in CDK7i-resistant melanoma cells

We compared the MM074^{CDK7i-R} and MM047^{CDK7i-R} gene expression programs to potentially identify a signature involved in drug tolerance that emerges as melanocytic-type cells undergo a phenotype switch and that is shared with the drug-resistant mesenchymal cells. This comparison focusing on genes commonly regulated during drug tolerance bypassing the much larger number of genes characterizing the phenotype switch *per se* identified the K7iRS genes. Merging these genes with a list of annotated transcription factors identified 16 common up-regulated transcription factors (TFs) in MM074^{CDK7i-R} and MM047^{CDK7i-R} (Fig EV2A). Analysis of their expression in RNA-seq data from melanoma cells showed that only 4 were significantly more expressed in the CDK7i-resistant MM029, MM099, MM074^{CDK7i-R}, and MM047^{CDK7i-R} cells, compared to CDK7i-sensitive cells (Fig EV2B). Of these, only GATA6 was significantly overexpressed in primary melanoma *vs* nevi (Fig EV2C). We confirmed by RT–qPCR and immuno-blot higher levels of GATA6 mRNA and GATA6 protein, respectively, in the CDK7i-insensitive cells (Fig 3A and B). We also noted that

Figure 2. Exposure to CDK7i induces melanoma dedifferentiation.

- Volcano plots were used to demonstrate differentially expressed genes as determined by RNA-seq in either MM047^{CDK7i-R} *vs* MM047 (top), MM074^{CDK7i-R} *vs* MM074 (middle), or MM074^{BRAFi-R} *vs* MM074 (bottom). Red dots show significantly over-represented (top) or under-represented (bottom) RNAs in drug-resistant cells compared to parental cells. All data were evaluated with the DESeq2 R package. The value for a given gene is the normalized gene expression value relative to the mean of all samples belonging to the same condition.
- Proportional Venn diagrams indicating the number of up-regulated (top) and down-regulated (bottom) genes in MM047^{CDK7i-R} and MM074^{CDK7i-R} compared to the parental MM047 and MM074, respectively. The number of genes overlapping between the datasets is indicated. 261 genes were found up-regulated and 241 down-regulated in MM047^{CDK7i-R} and MM074^{CDK7i-R}. Hypergeometric *P*-value is indicated.
- Genes characterizing the melanocytic-type and mesenchymal-like transcription signatures (Widmer *et al*, 2012) have been plotted on a heatmap and are shown in relation to their expression in different melanoma cells. RPKM values are represented as z-score. The group of genes related to pigmentation has been highlighted in red. The color key shows the log₂ expression values. Yellow color stands for high expression and dark violet for low expression.
- Protein lysates from MM074, MM074^{BRAFi-R}, or MM074^{CDK7i-R} were immuno-blotted for indicated proteins. Molecular sizes of the proteins are indicated (kDa). The numbers below the gel lanes represent relative protein level, which was determined from the band intensity using ImageJ software and normalized to each relative vinculin control.

Source data are available online for this figure.

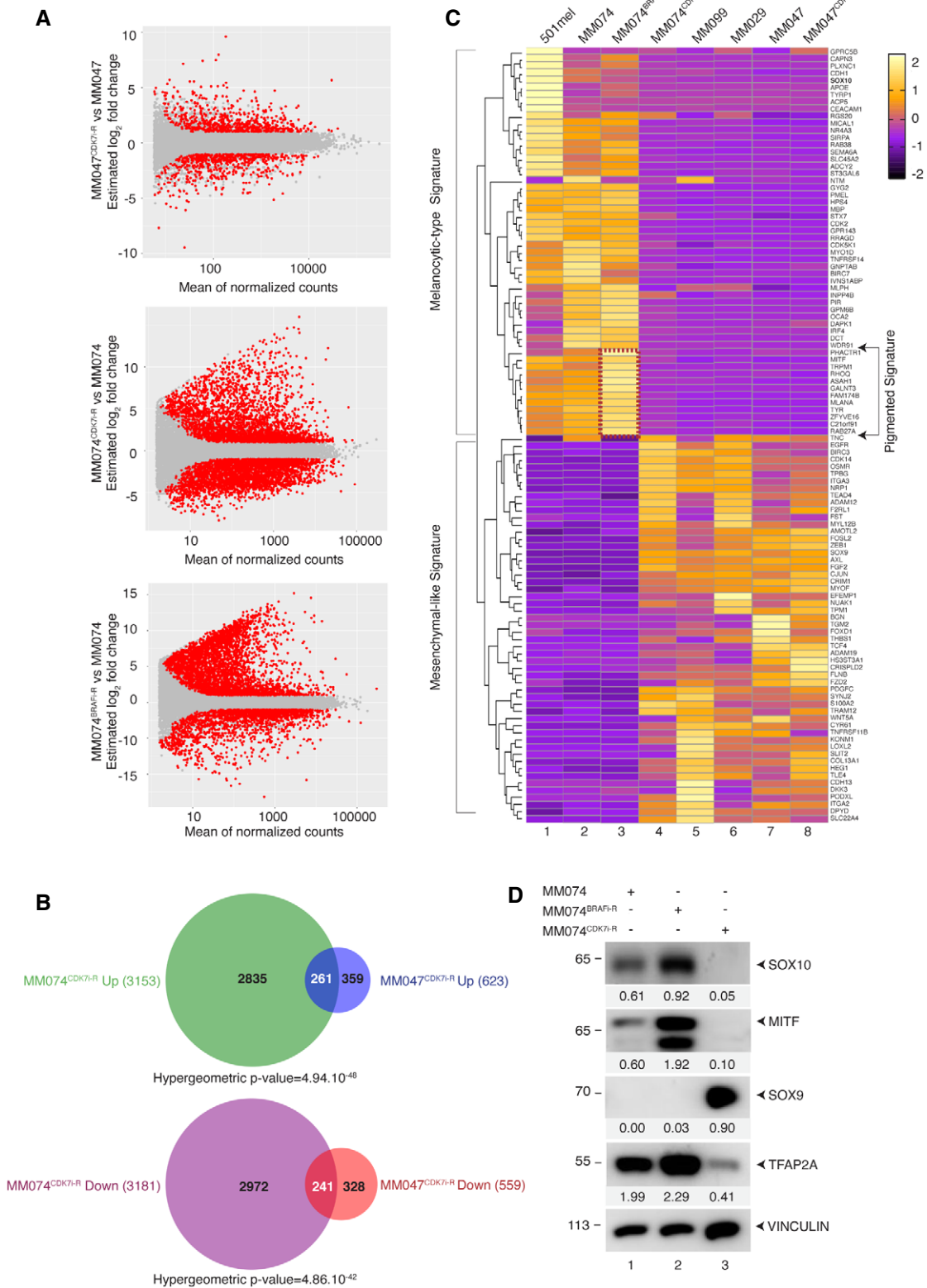


Figure 2.

GATA6 protein in MM047-sensitive cells was much lower than in the tolerant MM029 and MM099 cells and was potently induced in MM047^{CDK7-R} (Fig 3B).

We then analyzed the transcriptomic profiles of the CDK7-insensitive mesenchymal-like MM099 cells in which GATA6 was depleted using siRNA and observed a significant down-regulation of

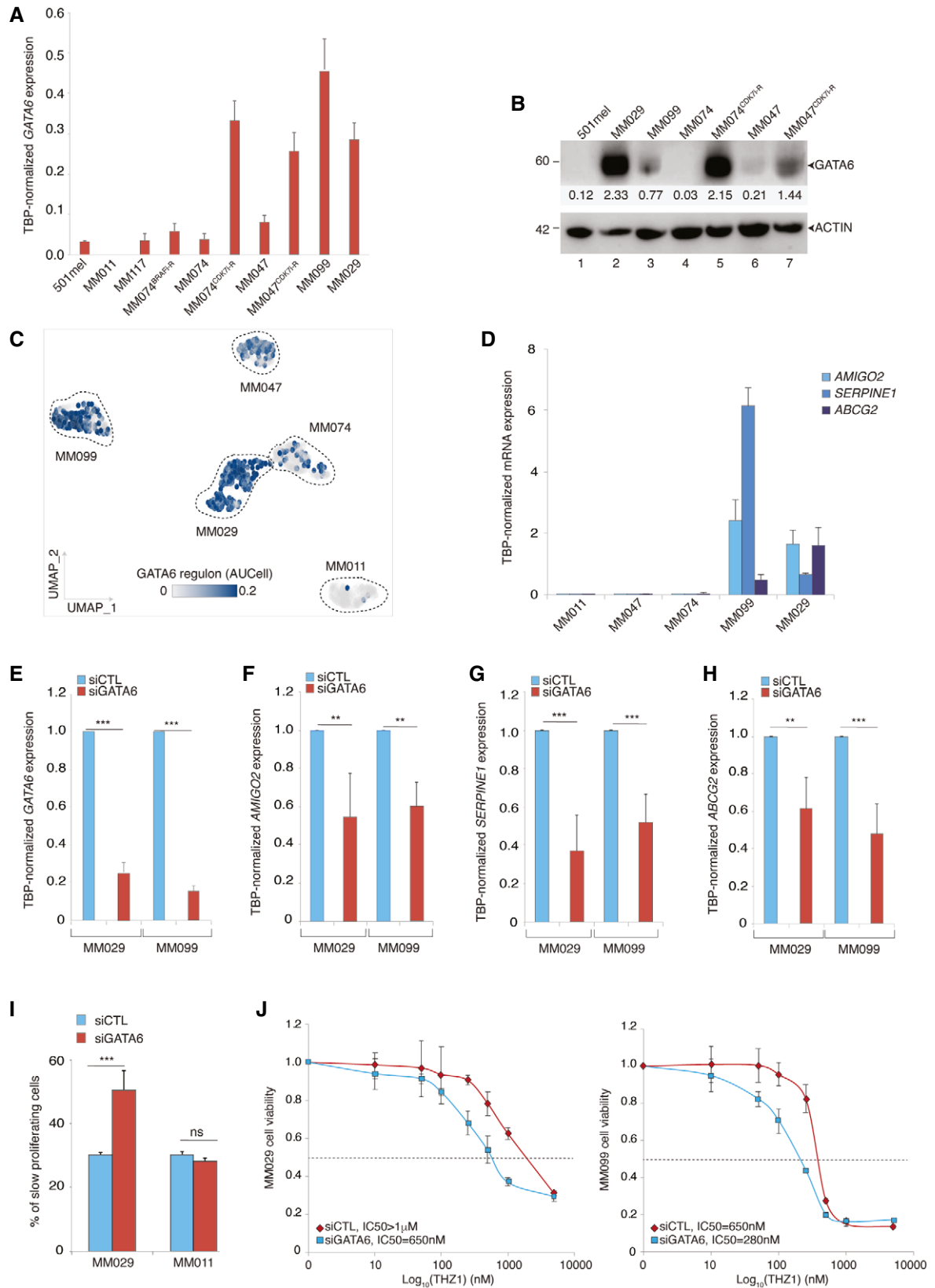


Figure 3.

Figure 3. GATA6 and its regulon are expressed in CDK7i-tolerant melanoma cells.

- A qRT-PCR analysis showing average *TBP*-normalized expression of *GATA6* in the indicated cells.
- B Protein lysates from the indicated cells were immuno-blotted for the indicated proteins. Molecular sizes of the proteins are indicated in kDa. The numbers below the gel lanes represent relative protein level, which was determined from the band intensity using ImageJ software and normalized relative to each relative actin control.
- C UMAP (Uniform Manifold Approximation and Projection) dimension reduction representative of *GATA6* regulon expression in MM011, MM029, MM047, MM074, and MM099 from Wouters dataset (Wouters *et al*, 2020). UMAP is colored according to the continuous *GATA6* AUCell values (from 0 to 0.2).
- D qRT-PCR analysis showing average *TBP*-normalized expression of *AMIGO2*, *SERPINE1*, and *ABCG2* in the indicated cells.
- E–H qRT-PCR analysis showing average *TBP*-normalized expression of *GATA6* (E), *AMIGO2* (F), *SERPINE1* (G), and *ABCG2* (H) in the indicated cells treated with either siCTL or si*GATA6* for 72 h.
- I MM011 and MM029 were treated with either siCTL or si*GATA6* for 72 h. Cell proliferation was analyzed using CellTrace staining and flow cytometry in the indicated cell lines, and the % of slow proliferating cells is shown for each condition.
- J MM029 (left) and MM099 (right) were pre-treated with either siCTL or si*GATA6* for 48 h and treated with increasing concentrations of THZ1 for 72 h. Mean growth is shown relative to vehicle (DMSO)-treated cells.

Data information: In (A, D–J), data are presented as mean values + SD for six replicates ($n = 6$). The *P*-value (Student's *t*-test) is indicated, ** < 0.01, *** < 0.005, and ns, non-significant.

Source data are available online for this figure.

86 genes following *GATA6* silencing (defined below as “*GATA6* regulon”) (Dataset EV2). We next examined expression of the *GATA6* regulon in single-cell transcriptomic data recently obtained from MM011, MM029, MM047, MM074, and MM099 (Wouters *et al*, 2020). The *GATA6* regulon was more enriched in CDK7i-insensitive MM099 and MM029 cells compared to the others (Fig 3C). Within the *GATA6* regulon, we identified genes whose function was previously defined as important for melanoma such as the *Adhesion Molecule with Ig like domain 2* (*AMIGO2*) (Fontanals-Cirera *et al*, 2017) and the *SERPINE family E member 1* (*SERPINE1*) (Klein *et al*, 2012) together with genes contributing to multidrug resistance in cancer cells such as the efflux pump *ATP Binding Cassette Subfamily G member 2* (*ABCG2*) (Robey *et al*, 2018). RT-qPCR showed that expression of these genes was significantly higher in the CDK7i-resistant MM099 and MM029 cells compared to MM011, MM047, and MM074 (Fig 3D). As in MM099, *GATA6* depletion in MM029 decreased expression of *AMIGO2*, *SERPINE1*, and *ABCG2* (Fig 3E–H). Furthermore, *GATA6* depletion diminished MM029 proliferation compared to MM011 (Figs 3I and EV2D) and sensitized MM029 and MM099 to CDK7i (Figs 3J and EV2D). We also tried to overexpress *GATA6* in melanocytic-like cells; however, its expression was toxic in these cells, leading to cell cycle arrest that compromised the isolation of stably expressing clones. Therefore, we overexpressed *GATA6* in the mesenchymal-like MM047 cells and obtained stable expression of *GATA6* (Fig EV2E). Ectopic expression of *GATA6* induced expression of *ABCG2*, *AMIGO2*, and *SERPINE1* (Fig EV2E and F) and increased resistance to CDK7i (Fig EV2G). These data suggested that *GATA6* coordinated the expression of a set of genes specifically expressed in drug-tolerant mesenchymal-like melanoma cells and required for proliferation/survival and drug resistance.

ABCG2 is involved in tolerance to CDK7i and BRAFi in melanoma cells

The above data suggest that up-regulation of *ABCG2* expression by *GATA6* in mesenchymal-like melanoma cells may promote CDK7i resistance. RNA-seq data from melanoma tumors and *in situ* mRNA hybridization of melanoma tumor sections

demonstrated higher expression of *ABCG2* in cutaneous metastatic melanoma compared to primary tumors (Fig EV3A and Appendix Fig S2). Three ABC transporters (*ABCG2*, *ABCB1*, and *ABCC3*) were up-regulated in MM047^{CDK7i-R} and/or MM074^{CDK7i-R} (Fig EV3B and C), but only *ABCG2* was overexpressed in the CDK7i-insensitive MM099 and MM029 (Fig 4A and B). Depletion of *ABCG2* using siRNA (Fig EV3D) significantly sensitized MM099 and MM029 to CDK7i (Fig 4C and D). Interestingly, depletion of *ABCG2* also sensitized MM099 cells to BRAFi (Fig 4E), showing the potential pleiotropic impact of this efflux pump on drug resistance. Consistently, decrease of *ABCG2* in MM029 cells did not impact their sensitivity to BRAFi since they harbored the vemurafenib-resistant BRAF^{V600K} mutation (Fig 4F). Taken together, these data suggested that the ABC transporter *ABCG2* played a significant role in tolerance to CDK7i and BRAFi in melanoma cells.

CDK7 regulates expression of MITF and SOX10

We investigated the regulation of *GATA6* regulon that was repressed in melanocytic melanoma cells and activated by chronic exposure to CDK7i. Previous work suggested that CDK7 occupied SEs regulating *MITF* and *SOX10* expression in melanoma cells (Eliades *et al*, 2018), but the presence of CDK7 at *MITF*/*SOX10*-associated super-enhancers was not observed so far. We performed ChIP-seq chromatin profiling of CDK7 using 501mel where the CDK7 locus was tagged with a Biotin-3xFlag tag by CRISPR/Cas9 genome editing (501mel^{BIO-FLAG:CDK7}) (Appendix Fig S3). FLAG ChIP-seq identified numerous CDK7-binding sites throughout the *MITF* locus and of its transcriptional activator *SOX10* (Fig 5A and B). CDK7 occupancy co-localized with H3K27ac, binding of *MITF* and/or of *SOX10*, BRG1, or H2AZ, all characterizing SE elements. A short 24 h CDK7i treatment impaired *MITF* and *SOX10* expression in 501mel, whereas exposure to BETi JQ1 had no effect (Fontanals-Cirera *et al*, 2017) (Fig 5C and D and Appendix Fig S4). Interestingly, decrease of *MITF* and *SOX10* following CDK7i occurred in parallel with increased expression of *GATA6* (Fig 5E). Moreover, expression of *CDK7*, *MITF*, and *SOX10* anti-correlated with that of *GATA6* in published RNA-seq data from human patient cutaneous melanoma (SKCM from TCGA) (Appendix Fig S5A).

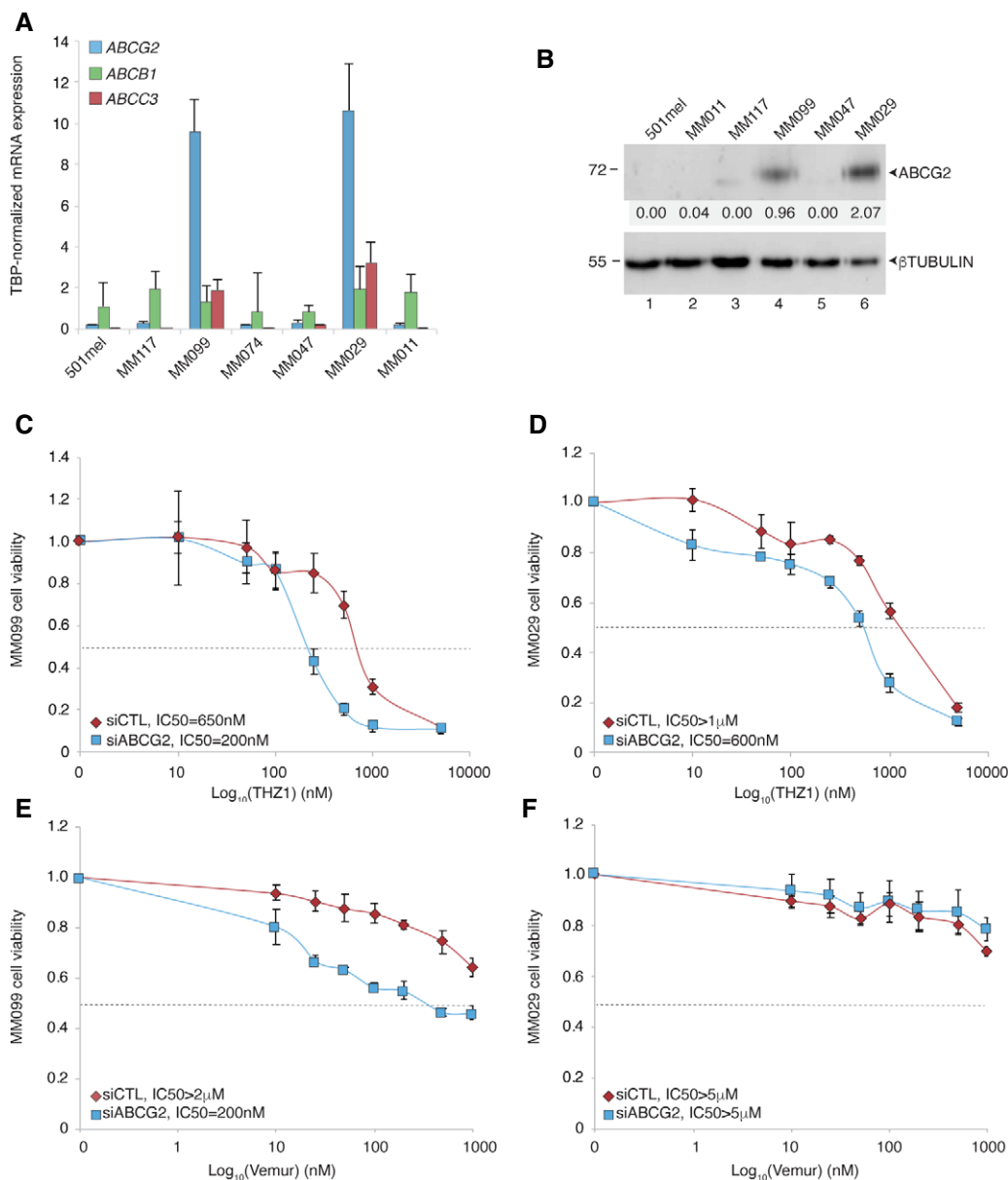


Figure 4. ABCG2 is involved in multidrug tolerance in melanoma cells.

A qRT-PCR analysis showing average TBP-normalized expression of ABCB1, ABCC3, and ABCG2 in the indicated cells.

B Protein lysates from the indicated cells were immuno-blotted for the indicated proteins. Molecular masses of the proteins are indicated in kDa. The numbers below the gel lanes represent relative protein level, which was determined from the band intensity using ImageJ software and normalized to each relative beta-tubulin control.

C, D MM099 (C) and MM029 (D) were pre-treated with either siCTL or siABCG2 as indicated and treated with increasing concentrations of THZ1 for 72 h. Mean growth is shown relative to vehicle (DMSO)-treated cells.

E, F MM099 (E) and MM029 (F) were pre-treated with either siCTL or siABCG2 as indicated and treated with increasing doses of vemurafenib for 72 h. Mean growth is shown relative to vehicle (DMSO)-treated cells.

Data information: In (A), data are presented as mean values + SD for six replicates (n = 6). In (C-F), data are presented as mean values + SD for three replicates (n = 3). IC50 for each cell line is indicated.

Source data are available online for this figure.

SOX10 silencing induces release of GATA6 regulon expression

The above data suggested that decreased MITF and/or SOX10 expression may induce GATA6 expression. To test this, we depleted SOX10

with siRNA in 501mel cells and observed a significant decrease of MITF and induction of GATA6 expression (Fig 6A and Appendix Fig S5B). In agreement, bioinformatic analyses of published scRNA-seq performed at different times after SOX10 depletion in melanocytic-like

MM074 cells (Wouters *et al*, 2020) showed concomitant activation of the GATA6 regulon (Fig 6B and C and Appendix Fig S5C). We observed that progressive *SOX10* and *MITF* down-regulation (Fig 6D

and E) correlated with concomitant up-regulation of *GATA6*, *ABCG2*, *SERPINE1*, and *AMIGO2* (Fig 6F–I). Altogether, these data showed an antagonism between MITF/SOX10 and GATA6 regulon in melanoma.

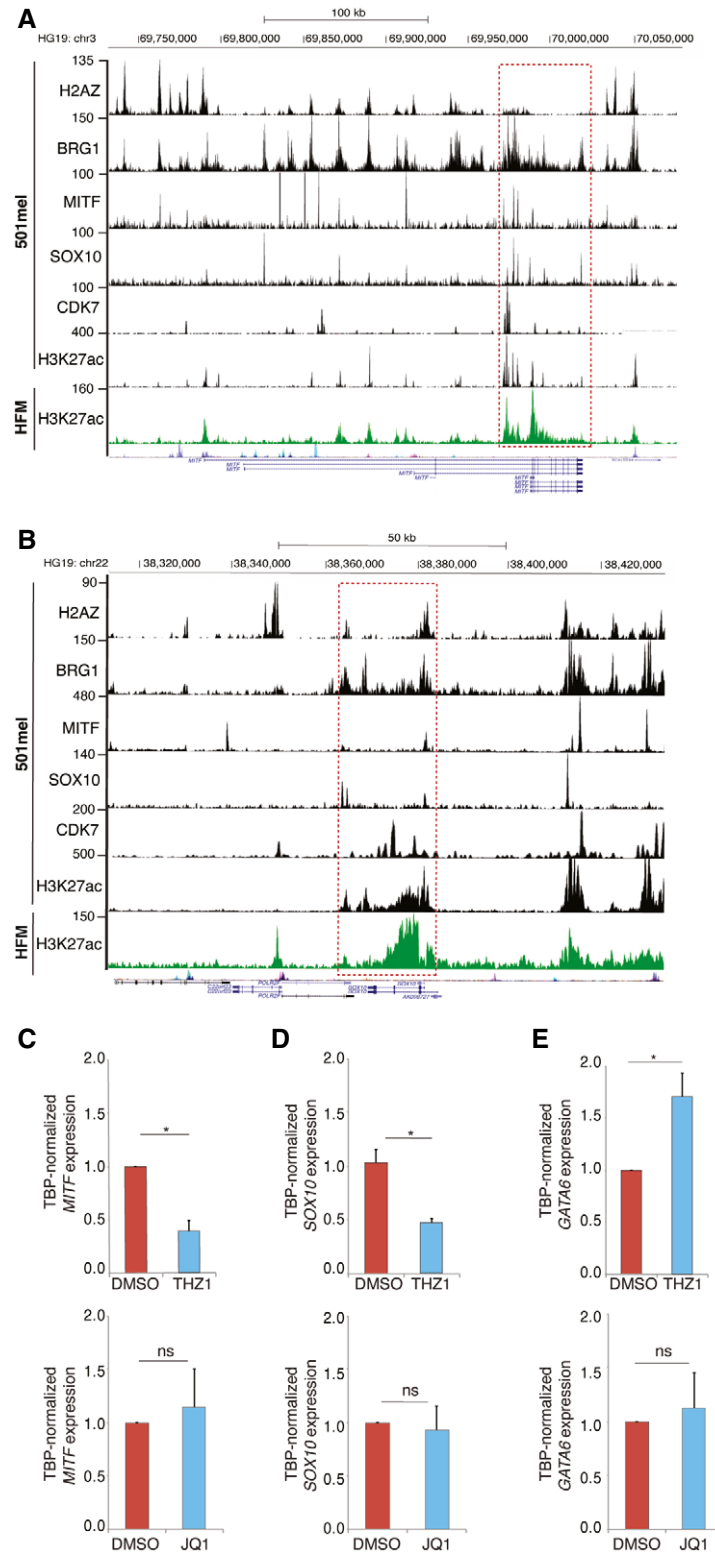


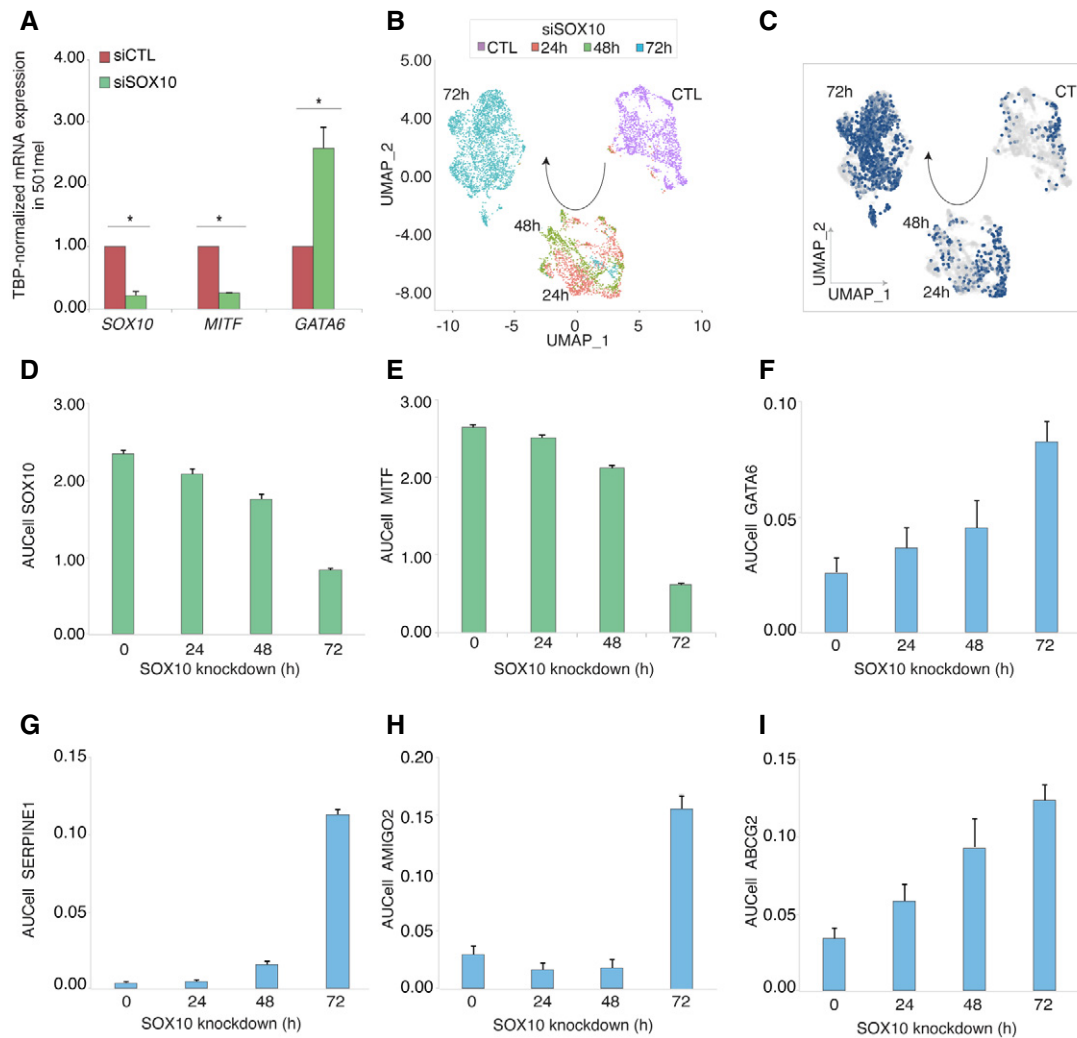
Figure 5.

Figure 5. CDK7i induced inhibition of MITF and SOX10 and release of GATA6 expression.

A, B Gene track of CDK7 occupancy at *MITF* (A) or *SOX10* (B) loci in 501mel^{BIO-FLAG:CDK7} cell line. Gene tracks of H2A.Z, BRG1, MITF, SOX10, and H3K27ac (GSE94488 and GSE61967) at the same loci in parental 501mel are indicated. SE is denoted by a red opened square. H3K27ac deposition is also shown in Hair Follicle Melanocytes (HFM) (GSE94488).

C–E qRT–PCR analysis showing average *TBP*-normalized fold expression of *MITF* (C), *SOX10* (D), and *GATA6* (E) in 501mel treated with either DMSO/THZ1 (50 nM) (upper) or DMSO/Q1 (10 μ M) (lower) for 24 h.

Data information: In (C–E), data are presented as mean values + SD for six replicates ($n = 6$). The *P*-value (Student's *t*-test) is indicated, * < 0.05.

**Figure 6. Loss of SOX10 and MITF releases GATA6 expression.**

A qRT–PCR analysis showing average *TBP*-normalized fold expression of *SOX10*, *MITF*, and *GATA6* in 501mel treated with either siCTL or siSOX10 for 48 h.

B Seurat UMAP of MM074 treated with siCTL or siSOX10 (24, 48, and 72 h post-treatment). The arrow indicated the trajectory from control to 72 h post-siSOX10 transfection.

C UMAP of AUCell *GATA6* regulon in MM074 shows that *GATA6* regulon is up-regulated along the trajectory from siCTL to 72 h post-siSOX10 treatment (GSE116237) (Wouters et al, 2020). The arrow indicated the trajectory from siCTL to 72 h post-siSOX10 transfection. We considered cell with *GATA6* regulon activity of AUCell > 0.15 as active (see Appendix Fig S5).

D–I Graphs showing the average expression of the *SOX10* (D), *MITF* (E), *GATA6* (F), *SERPINE1* (G), *AMIGO2* (H), and *ABCG2* (I) per individual melanoma cell measured by AUCell on MM074 at different time points post-transfection of siSOX10 (GSE116237) (Wouters et al, 2020).

Data information: In (A), data are presented as mean values + SD for six replicates ($n = 6$). The *P*-value (Student's *t*-test) is indicated, * < 0.05. In (D–I), data are presented as mean values + standard error of the mean (SEM) for six replicates ($n = 6$).

MITF drives direct transcriptional repression of GATA6

The above data suggested a direct mechanistic link between SOX10 and/or MITF and the repression of GATA6 in melanoma cells. ChIP-

seq did not reveal SOX10 binding at the GATA6 locus in 501Mel cells; however, a prominent MITF-binding site was observed in an intronic region of the GATA6 gene body (hereafter called “intGATA6r”, for intronic GATA6 locus region) containing potential

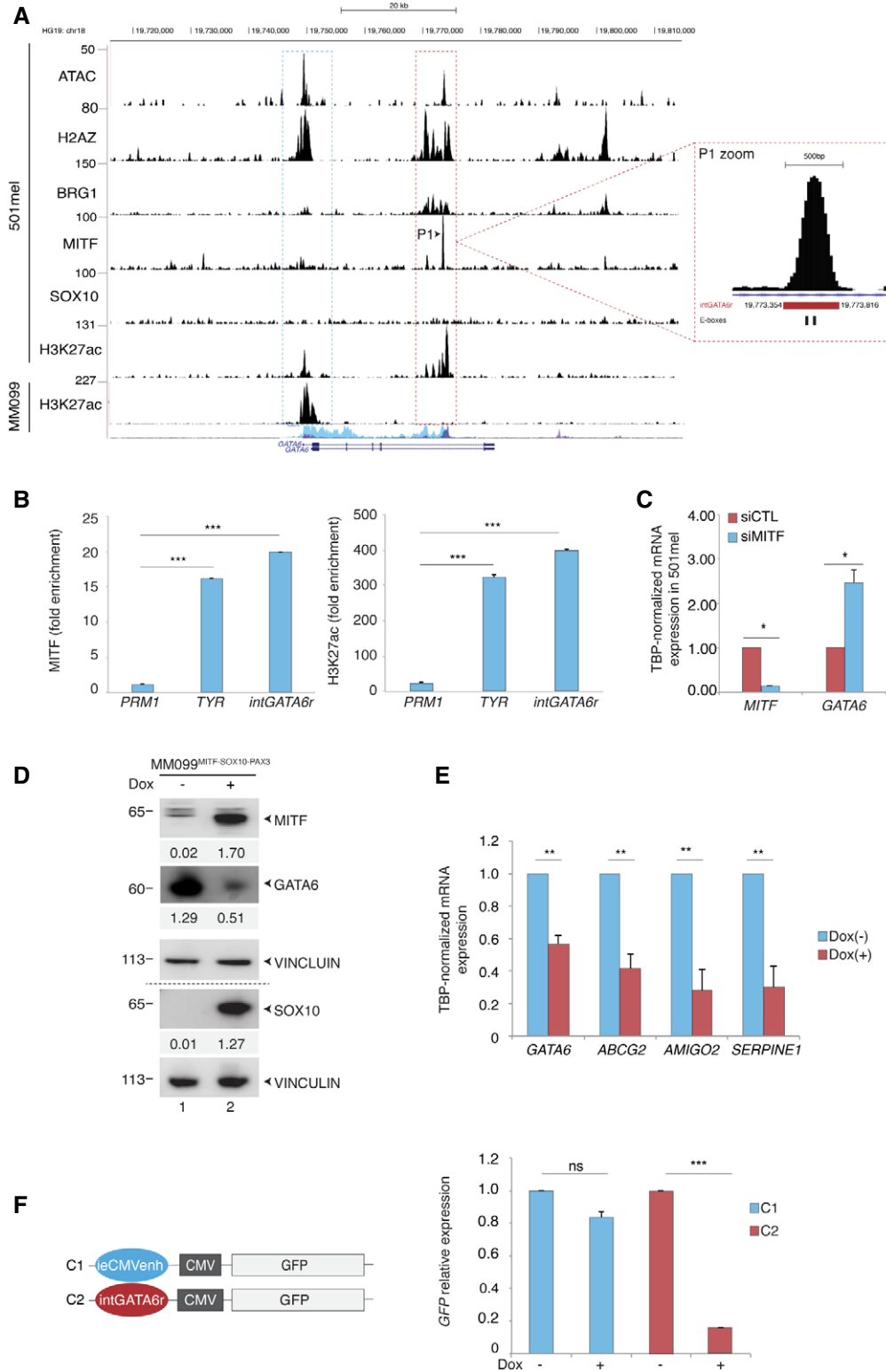


Figure 7.

Figure 7. MITF binds and represses the GATA6 locus.

- A ChIP-seq track of 3HA-MITF signal occupancy showing a significant MITF-binding peak (P1) in the GATA6 gene body in 501mel (GSE61967). Additional tracks indicate potential regulatory regions highlighted by ATAC-seq and H3K27ac, BRG1, SOX10, and H2A.Z deposition (GSE94488 and GSE61967). H3K27ac deposition is also shown in MM099 at the GATA6 locus. The scale bar indicates the size of the genomic region in kilobases (Kb). A magnification of the P1 region for MITF occupancy is shown in which the “intGATA6r” region is indicated in red and the two E-boxes in black.
- B ChIP qPCR experiment monitoring the fold enrichment (compare to control IgG) of MITF protein and H3K27ac mark at the “intGATA6r” region. *Proteamine 1 (PRM1)* and Tyrosinase (*TYR*) regulatory regions were used as negative and positive controls, respectively (Laurette et al, 2015).
- C qRT-PCR analysis showing average TBP-normalized fold expression of *MITF* and *GATA6* in 501mel treated with either siCTL or siMITF for 48 h.
- D MM099^{MITF-SOX10-PAX3} expressing inducible *MITF-SOX10-PAX3* genes was treated or not with doxycycline (1 µg/ml) for 24 h, and protein lysates were immuno-blotted for the indicated protein. The numbers below the gel lanes represent relative protein level, which was determined from the band intensity using ImageJ software and normalized relative to vinculin control.
- E qRT-PCR analysis showing average TBP-normalized fold expression of *GATA6*, *ABCG2*, *AMIGO2*, or *SERPINE1* in MM099^{MITF-SOX10-PAX3} treated or not with doxycycline (1 µg/ml) for 24 h.
- F Left panel: Schematic representation of pcDNA-ieCMVenh-CMV-GFP (C1) or pcDNA-intGATA6r-CMV-GFP (C2) reporter vectors. The ieCMVenh sequence in C1 was replaced by the “intGATA6r” sequence to generate C2. Right panel: qRT-PCR analysis showing average TBP-normalized fold expression of *GFP* in MM099^{MITF-SOX10-PAX3} transfected with C1 or C2 vectors for 48 h before treatment or not with doxycycline (1 µg/ml) for 24 h.

Data information: In (B, C, E), data are presented as mean values + SD for three biological triplicates. The *P*-value (Student's *t*-test) is indicated, * < 0.05, ** < 0.01, and *** < 0.001. In (F), data are presented as mean values + SD for three technical replicates (*n* = 6). The *P*-value (Student's *t*-test) is indicated, *** < 0.005 and ns, non-significant (> 0.05).

Source data are available online for this figure.

MITF-binding sites (E-box motifs) (Fig 7A) (Laurette et al, 2015). In addition, “intGATA6r” was enriched in H3K27ac, BRG1, and H2AZ, marks of enhancer elements. Interestingly, in MM099 where MITF is not expressed, intronic H3K27ac was lost, but rather replaced by strong H3K27ac labeling at the *GATA6* promoter, correlating with its high expression in these cells. ChIP-qPCR confirmed enrichment of MITF and H3K27ac at the “intGATA6r” region in 501mel (Fig 7B). In agreement with a role for MITF in *GATA6* repression, siMITF silencing in 501mel induced *GATA6* expression (Fig 7C and Appendix Fig S5B).

To determine whether MITF was able to transcriptionally repress *GATA6*, we generated MM099^{MITF-SOX10-PAX3} in which MITF, SOX10, and PAX3 expression could be induced by doxycycline (Dox) treatment (Fig 7D). We co-expressed MITF, SOX10, and PAX3 as we observed that the presence of SOX10 and PAX3 stabilized MITF in these cells. Following induction of MITF-SOX10-PAX3, *GATA6* mRNA expression was repressed and level of *GATA6* protein decreased (Fig 7D and E). Consequently, the expression of the *GATA6* regulon genes *ABCG2*, *AMIGO2*, and *SERPINE1* was inhibited (Fig 7E).

To establish its repressive role, the 500bp “intGATA6r” sequence was inserted upstream of the CMV promoter of the pcDNA-CMV vector to replace the immediate early CMV enhancer (“ieCMVenh”) in the context of a GFP reporter vector (Fig 7F, left panel). The reporter construct was transiently transfected into MM099^{MITF-SOX10-PAX3} with or without Dox-induced MITF-SOX10-PAX3 expression. While ieCMVenh-dependent GFP expression was barely affected by MITF-SOX10-PAX3 expression, the presence of the “intGATA6r” element upstream of the promoter strongly impacted expression of the GFP compared to cells that did not express MITF-SOX10-PAX3 (Fig 7F, right panel). Altogether, these data strongly suggested that MITF transcriptionally repressed *GATA6* by binding to a negative regulatory sequence located in an intronic region of *GATA6*.

GATA6 is expressed in MITF-low cells of human melanoma

Our *in vitro* data suggested that *GATA6* and its regulon may be expressed in MITF-low melanoma cells in human tumors. To test

this hypothesis, we first performed an immunohistological (IHC) examination of human tumor samples. Because MITF antibodies are poorly efficient in IHC, we rather detected its transcriptional activator SOX10. While *GATA6* was not observed in nevi and primary melanomas that showed high SOX10 expression (Fig 8A, panels a-d), it was highly expressed in a subpopulation of cells in cutaneous metastases that did not express SOX10 (Fig 8A, panels e-f). In line with the above data, analyses of public DNA microarray (Xu et al, 2008) or RNA-seq data (TCGA) consistently revealed higher expression of *GATA6* in metastatic melanoma compared with primary melanoma (Fig EV4A).

To further define which melanoma cell subtypes express *GATA6* and its regulon, we re-analyzed scRNA-seq data from a PDX tumor before and after BRAFi (dabrafenib) and MEKi (trametinib) combination treatment (Rambow et al, 2018). An unsupervised gene clustering analysis that included more cells than in the original published analyses detected 9 different cell subpopulation clusters (Fig 8B). GO analysis attributed the four previously well characterized phenotypes to clusters 1, 5, 7, and 8, specifically starved-like melanoma cells (SMC), pigmented, invasive and neural crest-stem cells (NCSC) characterized by many of the previously described genes of each signature (Fig 8C). We attributed two additional phenotypes to clusters 4 and 6 that we defined as “Mitotic” due to the high expression of late S-phase and G2 M phase genes and “IFN-active” (previously designated as Immune (Rambow et al, 2018)) due to the enriched expression of interferon response genes. Cluster 0 corresponded to MITF-intermediate proliferative cells, while no specific ontology could be assigned to clusters 2 and 3 that were characterized by high expression of mitochondrial or pseudo-genes, respectively, and were excluded from subsequent analyses.

The frequency of cells of each phenotype was then analyzed at the different phases defined by Rambow before and after MAPKi exposure (T0 is the drug-naïve phase, phases 1 and 2 are the minimal residual disease phase (MRD), and phase 3 is the development of drug resistance (Rambow et al, 2018)). As previously described, an increase in SMC, pigmented and NCSC at minimal residual disease (MRD) phases 1 and/or 2 was observed (Fig EV4B), while the frequency of mitotic cells was strongly reduced in phases 1 and

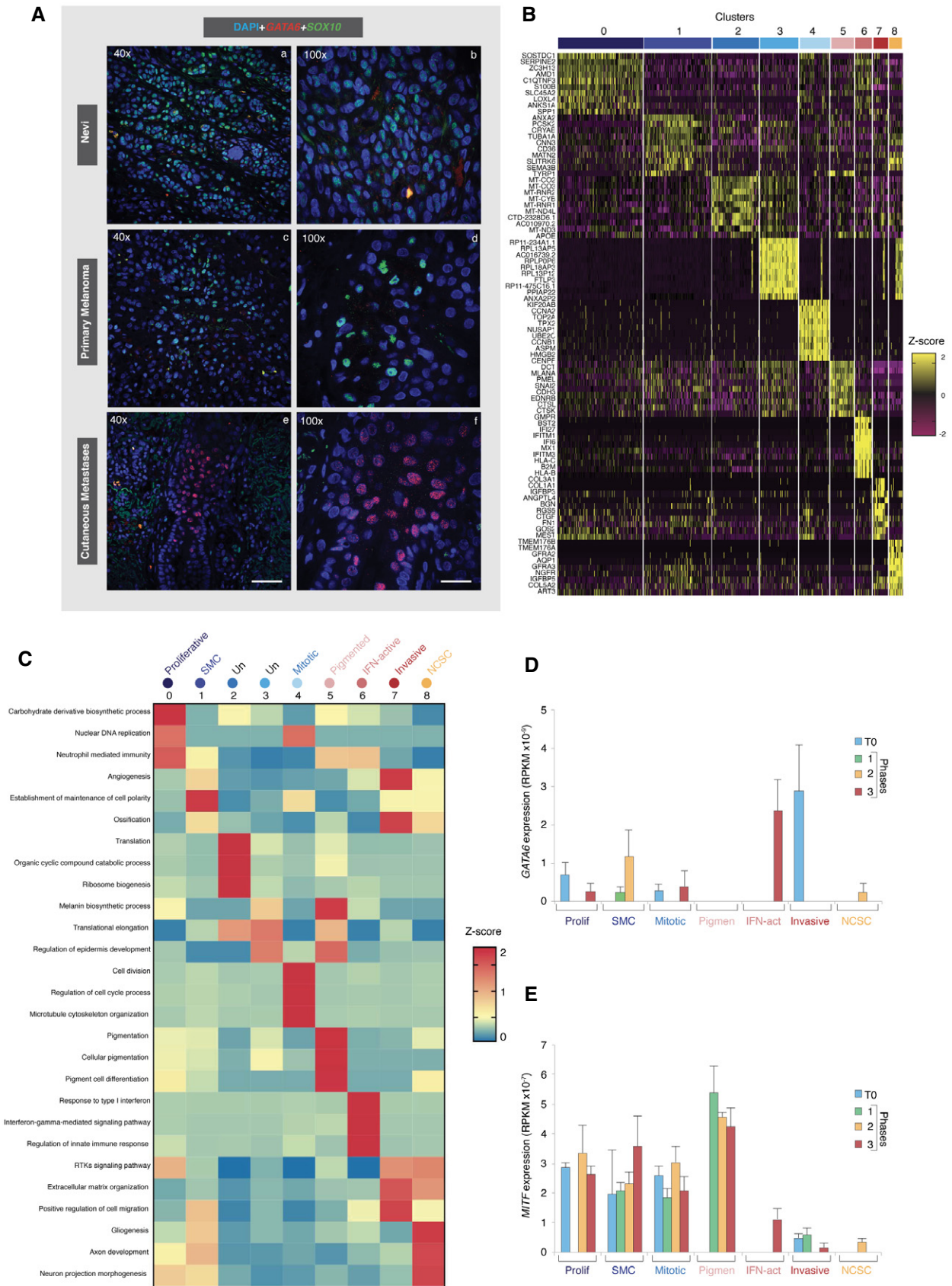


Figure 8.

Figure 8. GATA6 is expressed in MITF-low melanoma cells *in vivo*.

- A Tumor sections were immuno-labeled (IHC) with anti-GATA6 (red) and anti-SOX10 (green) antibodies, and images were captured by confocal microscopy at the indicated magnification. We analyzed six tumor sections of metastases and observed significant GATA6 expression in only one of them. Scale bar 250 μ m for 40 \times and 100 μ m for 100 \times .
- B Seurat cluster heatmap was generated from published scRNA-seq performed on PDX tumor ($n = 674$ cells) (GSE116237) (Rambow *et al*, 2018). The heatmap shows 9 different clusters into which the cells can be divided according to the expression of different referenced genes (Z-score). The top 10 genes are indicated in the left for each cluster.
- C GO was used to analyze the genes characterizing each cluster identified above. The average *P*-value was retrieved for each cluster taking the 3 best GO per cluster, and then, z-score ((*P*-value of each biological process-average of *P*-value of each biological process)/standard deviation) was calculated. Clusters 2 and 3 were undefined (un).
- D, E Graphs showing the average expression of *GATA6* (D) and *MITF* (E) (RPKM) for each phenotype cluster in T0 (drug naïve) (blue), phases 1–2 (MDR) (green and yellow), and phase 3 (drug resistance) (red).

Data information: In (D, E), data are presented as mean values + SEM ($n = 6,574$ cells from 5 PDX).

2 but increased in the drug-resistance phase 3. The IFN-active cells were present uniquely in phase 3. MITF-intermediate proliferative cells were prevalent at the drug-naïve phase T0, but declined strongly in phase 1 before becoming more numerous in phases 2 and 3.

Analyses of GATA6 expression in the seven cell types during the defined phases indicated that GATA6 significantly emerged in cells displaying “Invasive” phenotype at T0, persisted at low levels in “SMC” cells during the MRD phase before re-emerging in cells with “IFN-active” phenotype during the drug-resistant phase 3 (Fig 8D). In contrast, MITF was expressed in cells with “SMC” or “Mitotic” phenotypes in T0, but showed essentially no expression in “Invasive” or “NCSC” cells and was strongest expressed in “Pigmented” cells with lower expression in the “IFN-active” cells at the drug-resistance phases (Fig 8E). The expression of GATA6 in “IFN-active” melanoma cells in the PDX prompted us to treat MM074 cells with the pro-inflammatory cytokine IFN γ . This treatment decreased expression of MITF and up-regulated expression of GATA6, c-JUN (Riesenberg *et al*, 2015), and the positive control PD-L1 at both mRNA (Fig EV4C) and protein levels (Fig EV4D). These data indicated an anti-correlation between MITF and GATA6 in cells from PDX tumors together with the emergence of GATA6 in MITF-low cells of the drug-resistance phase. This anti-correlation was recapitulated in cells treated with the pro-inflammatory cytokine IFN γ .

Discussion

In this work, we have shown that CDK7i sensitivity of melanoma cells was independent of driver mutation status, but strongly influenced by their phenotype. MITF-high melanocytic-type melanoma cells were highly sensitive to CDK7i, while MITF-low mesenchymal-like melanoma cells were largely insensitive. As shown before (Ennen *et al*, 2017; Wouters *et al*, 2020), mesenchymal-like MM099, MM029, and MM047 showed similar, but not identical signatures. Our current data show that MM047 differs from the MM099 and MM029 cells in its resistance to CDK7i. As each are primary cultures from different patients with a different natural history of the disease, differences between lines are only to be expected. Through the establishment of CDK7i-resistant cells from two different parental phenotypes, we defined a set of 261 genes reflecting the adaptation of melanoma cells to the exposure to CDK7i. Among these, we identified a network governed by GATA6 and containing genes such as

AMIGO2, involved in melanoma cell survival. GATA6 and its regulon were not only expressed in melanoma cells chronically exposed to CDK7i *in vitro*, but also more broadly in melanoma cells showing low expression of the lineage-specific markers SOX10 and MITF in tumors. We further observed that depletion of SOX10 or MITF proteins also activated GATA6-dependent genes, suggesting that the decommission of the CDK7-dependent SEs regulating MITF and SOX10 expression following CDK7i exposure (Eliades *et al*, 2018) is a key step in their activation. Our results also established that CDK7i more strongly inhibited *MITF* and *SOX10* expression in melanoma cells compared to BETi (Fontanals-Cirera *et al*, 2017), despite the presence of BRD4 at their corresponding SEs (Eliades *et al*, 2018), that may just be a collateral non-functional recruitment associated with strong enrichment of coactivators at SEs. Further evidence for the critical role of MITF/SOX10 in GATA6 repression comes from their ectopic expression in mesenchymal-like cells that inhibited GATA6 expression. We further identified a short regulatory sequence in a GATA6 intron that is bound by MITF and conferred MITF-driven transcriptional repression in a heterologous setting, a recognized criterion for *bone fide* repressor elements.

Consistent with our analysis showing GATA6 expression in both “invasive” and “IFN-active” PDX melanoma cells, IFN γ treatment of melanocytic cells repressed MITF/SOX10 leading to the concomitant activation of *GATA6* (Son *et al*, 2014). Since MITF has been shown to participate in stabilization of CDK7 in melanocyte-type melanoma cells (Seoane *et al*, 2019; Louphrasitthiphol *et al*, 2020), our data suggest a negative feedback loop where the progressive loss of MITF during melanoma progression and inflammation triggers decreased CDK7 protein levels that in turn promotes lower MITF expression leading to de-repression of GATA6 expression in MITF/CDK7-low melanoma cells (Fig EV5). In line with this model, a negative correlation between CDK7 and GATA6 was observed in human SKCM.

GATA6 is expressed in various normal tissues derived from the mesoderm and endoderm (Almalki & Agrawal, 2016). An oncogenic role for GATA6 has been proposed in various cancers including pancreatic cancer where its knockdown reduced cell proliferation and cell cycle progression (Sun & Yan, 2020). We show that the decrease of GATA6 impaired proliferation of MITF-low mesenchymal-like melanoma cells. Since GATA6 is expressed in normal adult tissues, it is unlikely that its targeting would lead to efficient therapy. However, identification of its downstream regulon genes may help to identify molecular targets in mesenchymal-like melanoma cells that could be exploited therapeutically to prevent

acquisition of metastatic and drug resistance potential. One of the GATA6 regulon genes, *AMIGO2*, has already been identified as targetable for metastatic melanoma (Fontanals-Cirera *et al.*, 2017). We observed that the GATA6-dependent multidrug transporter *ABCG2* is, at least in part, responsible for cross-resistance to targeted therapies in mesenchymal-like cells and is significantly overexpressed in metastatic melanoma tumors compared with primary tumors, suggesting that it may mediate ubiquitous cross-resistance to targeted therapies clinically.

Our results also clearly established a role for CDK7 in transcriptional reprogramming of melanoma cells. MITF-high melanoma cells exposed to CDK7i progressively lost melanocytic-type markers and acquired those of the undifferentiated mesenchymal-like state. In acquired CDK7i-resistant melanoma cells, we detected both a mesenchymal-like transcriptional signature and the acquisition of programs responsible for invasion. In apparent contrast, we observed that the acquired resistance of MITF-high melanoma cells to BRAFi was not accompanied by a loss of lineage-specific markers. In our hands, and as previously observed (Haq *et al.*, 2013) (Smith *et al.*, 2016), chronic exposure of melanocytic-type melanoma cells to escalating doses of BRAFi switched them to a highly pigmented state, which is likely a consequence of the increased MITF expression that we observed in these cells (Khaled *et al.*, 2010).

Finally, an increasing number of studies identified CDK7 as a therapeutic target in various cancers (Fisher, 2019). However, the phenotype reprogramming observed during prolonged exposure of melanoma cells to CDK7i illustrates the potential danger of targeting this kinase in cancers where EMT plays an important role in therapeutic resistance and metastasis, an issue that has not been fully investigated so far. Future studies should therefore take into consideration the potential of CDK7i treatment to promote emergence of mesenchymal-like cells and therapeutic resistance.

Materials and Methods

A full list of reagents including antibodies, commercial kits, and oligonucleotides is supplied in Appendix Table S1.

Patients

Gene expressions in tumors and nevi were retrieved from several previously published datasets (including TCGA) indicated in the figure legends.

Cell culture and treatment

Cells were grown in 5% CO₂ at 37°C in HAM-F10 (Gibco, Invitrogen) supplemented with 10% FCS and penicillin–streptomycin. Melanoma cell line 501mel was grown in 5% CO₂ at 37°C in RPMI w/o HEPES (Gibco, Invitrogen) supplemented with 10% FCS and gentamycin.

Cells were transfected with Lipofectamine RNAiMAX following the manufacturer's instructions with 25 nM of siRNA ON-TARGETplus SMARTPool (Horizon Discovery), and cells were harvested 48 and/or 72 h after transfection. All cell lines used were mycoplasma negative.

MM099^{MITF-SOX10-PAX3}, MM047^{GFP}, and MM047^{GATA6} cells were generated as followed. Lentiviral vectors pTET-SMP encoding human untagged MITF, SOX10, and PAX3 proteins, and pLenti-EF1a-GFP and pLenti-EF1-3xFLAG-GATA6 encoding for GFP and GATA6 proteins, respectively, were transduced in either MM099 or MM047 in the presence of polybrene, and cells were selected with 3 µg/ml of puromycin. Conditional expression of pTET vector was carried out by adding 1 µg/ml of doxycycline in the medium for at least 24 h.

Generation of CDK7i- and BRAFi-resistant cells

To generate CDK7i- or BRAFi-resistant cells, we chronically exposed the MM074 (BRAF^{V600E}) melanocytic-type cells to escalating doses of THZ1 or vemurafenib over several weeks. These treatments were carried out until the cells proliferated in drug concentrations equal to at least 5 times the original IC50 values, allowing us to generate stable MM074^{CDK7i-R} and MM074^{BRAFi-R} lines, respectively. In parallel, the MM047 (NRAS^{Q61R}) mesenchymal-like cells were chronically exposed to THZ1 following the same protocol to generate stable MM047^{CDK7i-R}. Once established, the resistance was permanent and drugs can be removed without affecting cell phenotype.

CRISPR/Cas9 editing of 501mel^{BIO-FLAG:CDK7}

A 501mel were co-transfected with vector px738 (encoding Cas9-HF-GFP and two guide RNAs targeting CDK7 locus) and construct m599 linear DNA fragment carrying homology regions to CDK7 locus and puromycin-P2A-BIO-FLAG-CDK7N-termsequence (Appendix Table S1) with transfection reagent FuGENE6. Twenty-four h later, single cells GFP positive were sorted in P96-well plates in the presence of puromycin (3 µg/ml) with cell sorter. Single clones were let grown and selected for 4–6 weeks and surviving ones screened for gene editing through PCR using Phusion High-Fidelity TAQ Polymerase using different combination of primers (F1, F5, R3, R4, R5, see Appendix Table S1). PCR-positive clones were finally further amplified to perform Western blot and Co-IPs validation.

Cell proliferation assay

To measure proliferation, cells were incubated first with CellTrace Violet according to the manufacturer's instructions. Cell proliferation was detected on a BD LSRFortessa™ Flow Cytometer. Data were analyzed with FlowJo software. To define slow proliferating cells, we proceeded as follows: We considered that slow proliferating cells represented the 30% of cells with the highest concentration of BV421 in the siCTL treatment. We then calculated the % of cells that had a concentration greater than or equal to this value after treatment with siRNA.

Reporter assay

The intGATA6r element was isolated by genomic PCR using Phusion High-Fidelity TAQ polymerase (Thermo Fisher) with specific primers (Appendix Table S1). To allow the cloning within pCDNA-GFP vector, the first PCR product was further amplified by PCR with primers carrying MluI and SmaI restriction sites at the 5' and 3', respectively (MluI_F and SmaI_R primers in Appendix Table S1).

The immediate early CMV enhancer (ieEnh) in the pCDNA-GFP vector (pCDNA-ieEnh-CMV-GFP) was then replaced with the intGATA6r element (pCDNA-intGATA6r-CMV-GFP).

MITF-SOX10-PAX3 expression was induced in MM099^{MITF-SOX10-PAX3} cells with doxycycline for 48 h, and cells were subsequently transfected with pCDNA-ieEnh-CMV-GFP or pCDNA-intGATA6r-CMV-GFP vectors for 24 h with FuGENE6 following the manufacturer's instructions. RNA was then collected for qPCR, and GFP protein signal was detected on cytofluorometer. FACS data were analyzed with FlowJo software.

Histology

Human tissue sections were de-paraffinized and dehydrated with Histosol and dilutions of ethanol (100, 90, 70, and 30%) and then rehydrated with demineralized water. Subsequently, sections were boiled in sodium citrate buffer (0.1 M citric acid, 0.1 M sodium citrate) for 15 min to unmask antigens. Alternatively, cells were grown on glass slides and fixed with 4% formaldehyde. Both tissues and cells were permeabilized with PBS and 0.1% Triton X-100. Blocking was done with 10% fetal bovine serum before incubation with primary antibodies.

In situ hybridization of *ABCG2* mRNA was performed using the RNAscope assay according to the manufacturer's instructions (ACDBio). Cells and tissue sections were counterstained with DAPI and visualized using confocal microscope Spinning disk Leica CSU W1. Probes' sequences were not provided by the manufacture.

EU incorporation assay

RNA labeling by EU incorporation was performed with Click-iT RNA Imaging kit following the manufacturer's protocol. EU signal intensity was quantified using imaging system.

Cell survival assay

Normal or transfected cells were seeded at 5,000 cells/well in a 96-well plate and treated with increasing concentrations of THZ1, vemurafenib, or trametinib. After 72 h of incubation, cells were treated with PrestoBlue reagent according to the manufacturer's instructions. The absorbance per well was measured with a microplate reader. The data were then analyzed using Prism8.

RT-qPCR

Total RNA was isolated from cells using a GenElute Mammalian Total RNA Miniprep kit (Sigma) and reverse-transcribed with SuperScript IV reverse transcriptase (Invitrogen). The quantitative PCR was done using LightCycler. The primer sequences for the different genes used in qPCR are indicated in Appendix Table S1. The mRNA expression of the various analyzed genes represents the ratio between values obtained from treated and untreated cells normalized with the housekeeping genes mRNA.

ChIP

Cells were grown on 15-cm plates and, once reached 80% of confluence, were fixed with PBS + 0.4% formaldehyde solution for

10 min. Fixation reaction was stopped with 2 M Glycin pH 8. Cells were then pelleted and suspended in lysis buffer (EDTA 10 mM, Tris-HCl pH8 50 mM, SDS 1%) and sonicated with Covaris E220 AFA power 200 Hz 6 cycles 200 s to get a DNA fragmentation between 500 and 200 bp. Chromatin was then diluted in 60 μ g aliquots with 8 volumes of ChIP dilution buffer (Tris-HCl pH8 16.7 mM, EDTA 1.2 mM, NaCl 167 mM, Triton X-100 1.1%, SDS 0.01%). The immuno-precipitations were done as follows. 1–5 μ g of antibody-chromatin was then captured with G protein sepharose beads (Sigma-Aldrich) 1 h at 4°C. Beads were washed 2 times with low salt buffer (Tris-HCl pH8 20 mM, EDTA 2 mM, NaCl 150 mM, Triton X-100 1%, SDS 0.1%), high salt buffer (Tris-HCl pH8 20 mM, EDTA 2 mM, NaCl 500 mM, Triton X-100 1%, SDS 0.1%), LiCl buffer (Tris-HCl pH8 500 mM, EDTA 1 mM, Na deoxycholate 1%, NP40 1%, LiCl 0.25 M), and TE buffer (Tris-HCl pH8 10 mM, EDTA 1 mM), and DNA was eluted 30 min at room temperature with Elution buffer (NaHCO₃ 0.1 M, SDS 1%). DNA was finally purified through phenol-chloroform, re-suspended in 100 μ l of water, and analyzed by qPCR using a set of primers indicated in Appendix Table S1.

RNA-seq

RNA-seq was performed as previously described (Laurette *et al*, 2019). Reads were preprocessed in order to remove adapter and low-quality sequences (Phred quality score below 20). After this preprocessing, reads shorter than 40 bases were discarded for further analysis. These preprocessing steps were performed using cutadapt version 1.10. Reads were mapped to rRNA sequences using bowtie version 2.2.8, and reads mapping to rRNA sequences were removed for further analysis. Reads were mapped onto the hg19 assembly of Homo sapiens genome using STAR version 2.5.3a. Gene expression quantification was performed from uniquely aligned reads using htseq-count version 0.6.1p1, with annotations from Ensembl version 75 and "union" mode. Only non-ambiguously assigned reads have been retained for further analyses. Read counts have been normalized across samples with the median-of-ratios method (Anders & Huber, 2010). Differential gene expression analysis was performed using the methodology implemented in the Bioconductor package DESeq2 version 1.16.1 (Love *et al*, 2014). *P*-values were adjusted for multiple testing by the method proposed by Benjamini and Hochberg (Benjamini & Hochberg, 1995). Deregulated genes were defined as genes with $\log_2(\text{foldchange}) > 1$ or < -1 and adjusted *P*-value < 0.05 . Heatmaps were generated with the R package pheatmap v1.0.12.

ChIP-seq

Purified DNA fragments for ChIP-seq were prepared by using the ChIP-IT High Sensitivity Kit (Active Motif) and the related antibodies. ChIP-seq was performed on an Illumina sequencer as single-end 50 base reads following Illumina's instructions. Image analysis and base calling were performed using RTA 1.17.20 and CASAVA 1.8.2. Reads were mapped onto the hg19 assembly of the human genome. Peak detection was performed using MACS (<https://github.com/macs3-project/MACS>) under settings where the input fraction was used as negative control. Peaks detected were annotated using

HOMER (<http://biowhat.ucsd.edu/homer/ngs/annotation.html>) as well as TSS protein enrichment comparison. Quantitative comparison of RNA Pol II gene body enrichment was performed using seqMINER (<http://bips.u-strasbg.fr/seqminer/>). As reference coordinates, we used the MACS-determined peaks or the annotated TSS/TTS of human genes as defined by RefSeq database. Sequence enrichment was performed using RSAT (<http://rsat.sb-roscoff.fr>) with MACS-determined peaks as reference.

Analysis of scRNA-seq data from short-cultured melanoma cells

After being downloaded, raw reads from scRNA-seq from MM011, MM029, MM047, MM074, and MM099 (Wouters *et al*, 2020) were processed using CellRanger (v 3.1) to align on the hg19 human genome, remove unexpressed genes, and quantify barcodes and UMIs. Data were then analyzed in R (v4.0.2) with Seurat v3.2.0 following the recommended workflow. Cells were filtered for feature count ranging from 120 to 2,000 and percentage of mitochondrial reads < 15%. Counts were normalized with the “LogNormalize” method and data scaled to remove unwanted sources of variation (UMI count and mitochondrial reads). The number of principal components to use was determined from the Jackstraw plots. Clustering was performed on variable features using the 25 most significant principal components and a resolution of 1.15. Regulome analyses of active transcription factors were performed using the SCENIC v1.1.2.2 package. Transcription factor activities were visualized on the UMAP using AUCell or as heatmaps using the R package pheatmap. Trajectory on the UMAP projection was resolved by monocle3 v0.2.0.

Analysis of scRNA-seq from PDX

Expression matrix with row reads counts for the single-cell experiment was retrieved from GEO (GSE116237). Then, data were normalized and clustered using the Seurat software package version 3.1.4 (Butler *et al*, 2018) in R version 3.6.1. Data were filtered, and only genes detected in at least 3 cells and cells with at least 350 detected genes were kept for further analysis. Expression of 26,661 transcripts in 674 cells was quantified. To cluster cells, read counts were normalized using the method “LogNormalize” of the Seurat function NormalizeData. It divides gene expression counts by the total expression, multiplies this by a scale factor (10,000 was used), and log-transforms the result. Then, 2,000 variable features were selected with the variance stabilizing transformation method using the Seurat function FindVariableGenes with default parameters. Integrated expression matrices were scaled (linear transformation) followed by principal component analysis (PCA) for linear dimensional reduction. The first 20 principal components (PCs) were used to cluster the cells with a resolution of 0.5 and as input to tSNE to visualize the dataset in two dimensions. The Bioconductor package AUCell v 1.6.1 (Aibar *et al*, 2017) was used to assess whether some cells from the Rambow dataset were enriched in gene sets of interest. AltAnalyze was used for the supervised clustering of TCGA samples (Olsson *et al*, 2016).

Gene ontology

Gene ontology was performed using Metascape software developed by (Zhou *et al*, 2019).

Quantification and statistical analysis

Statistical details of experimental can be found in figure legends or in the methods details. Hypergeometric distribution tests for the Venn diagrams were performed using: <https://systems.crump.ucla.edu/hypergeometric/>.

Data availability

The datasets produced in this study are available in the following databases:

Access numbers for data generated in this paper are as follows:

ChIP-Seq data CDK7: Gene expression Omnibus GSE158118.

<https://www.ncbi.nlm.nih.gov/geo/query/acc.cgi?acc=GSE158118>

RNA-seq data CDK7i cells: Gene expression Omnibus GSE158119.

<https://www.ncbi.nlm.nih.gov/geo/query/acc.cgi?acc=GSE158119>

RNA-seq data: Gene expression Omnibus GSE164431.

<https://www.ncbi.nlm.nih.gov/geo/query/acc.cgi?acc=GSE164431>.

Expanded View for this article is available online.

Acknowledgments

We thank the IGBMC antibody and cell culture facilities, Prof D. Lipsker, and the staff of the Strasbourg University Hospital dermatology clinic for tumor sections and Dr Ghanem Ghanem and J-C Marine for providing us the MM-series melanoma cultures. This study was supported by the Institut National Du Cancer (INCa) (2015-9378 and 2017-11537), the Ligue contre le Cancer (Equipe labélisée 2019, FC and équipe labélisée 2018, ID) and the ANR (START-2021), the ANR-10-LABX-0030-INRT, a French State fund managed by the Agence Nationale de la Recherche under the frame program Investissements d’Avenir ANR-10-IDEX-0002-02. Sequencing was performed by the IGBMC GenomEast platform, a member of the “France Génomique” consortium (ANR-10-INBS-0009). PB is supported by the Ligue contre le Cancer. M.C is supported by the Fondation pour la Recherche Médicale.

Author contributions

PB, ID, and FC conceived the study. PB, ID, FC, and EC analyzed the data. PB generated the resistant cells and performed the RNA-seq and the IH staining. SL, GD, BV, and PB, performed the bioinformatics analyses. PB, MC, and CMGR performed the survival assays. EC, FP, PB, and MC performed the RT-qPCR and the WB. JS performed the EU staining. NS performed the IFN γ experiments. CB provided a valuable technical assistance. JME provided valuable materials. FC and ID wrote the manuscript with input from EC.

Conflict of interest

The authors declare that they have no conflict of interest.

References

- Aibar S, González-Blas CB, Moerman T, Huynh-Thu VA, Imrichova H, Hulselmans G, Rambow F, Marine J-C, Geurts P, Aerts J *et al* (2017) SCENIC: single-cell regulatory network inference and clustering. *Nat Methods* 14: 1083–1086
- Alekseev S, Nagy Z, Sandoz J, Weiss A, Egly JM, Le May N, Coin F (2017) Transcription without XPB establishes a unified helicase-independent

- mechanism of promoter opening in eukaryotic gene expression. *Mol Cell* 65: 504–514
- Almalki SG, Agrawal DK (2016) Key transcription factors in the differentiation of mesenchymal stem cells. *Differentiation* 92: 41–51
- Anders S, Huber W (2010) Differential expression analysis for sequence count data. *Genome Biol* 11: R106
- Arozarena I, Wellbrock C (2019) Phenotype plasticity as enabler of melanoma progression and therapy resistance. *Nat Rev Cancer* 19: 377–391
- Badal B, Solovyov A, Di Cecilia S, Chan JM, Chang LW, Iqbal R, Aydin IT, Rajan GS, Chen C, Abbate F et al (2017) Transcriptional dissection of melanoma identifies a high-risk subtype underlying TP53 family genes and epigenome deregulation. *JCI Insight* 2: e92102
- Benjamini Y, Hochberg Y (1995) Controlling the false discovery rate: a practical and powerful approach to multiple testing. *J R Stat Soc Ser B Methodol* 57: 289–300
- Berico P, Coin F (2018) Is TFIIH the new Achilles heel of cancer cells? *Transcription* 9: 47–51
- Brose MS, Volpe P, Feldman M, Kumar M, Rishi I, Cerrero R, Einhorn E, Herlyn M, Minna J, Nicholson A et al (2002) BRAF and RAS mutations in human lung cancer and melanoma. *Cancer Res* 62: 6997–7000
- Butler A, Hoffman P, Smibert P, Papalexi E, Satija R (2018) Integrating single-cell transcriptomic data across different conditions, technologies, and species. *Nat Biotechnol* 36: 411–420
- Cao K, Shilatfard A (2014) Inhibit globally, act locally: CDK7 inhibitors in cancer therapy. *Cancer Cell* 26: 158–159
- Carreira S, Goodall J, Denat L, Rodriguez M, Nuciforo P, Hoek KS, Testori A, Larue L, Goding CR (2006) Mitf regulation of Dia1 controls melanoma proliferation and invasiveness. *Genes Dev* 20: 3426–3439
- Chipumuro E, Marco E, Christensen C, Kwiatkowski N, Zhang T, Hatheway C, Abraham B, Sharma B, Yeung C, Altabef A et al (2014) CDK7 inhibition suppresses super-enhancer-linked oncogenic transcription in MYCN-driven cancer. *Cell* 159: 1126–1139
- Christensen C, Kwiatkowski N, Abraham B, Carretero J, Al-Shahrouf F, Zhang T, Chipumuro E, Herter-Sprie G, Akbay E, Altabef A et al (2014) Targeting transcriptional addictions in small cell lung cancer with a covalent CDK7 inhibitor. *Cancer Cell* 26: 909–922
- Compe E, Egly JM (2016) Nucleotide excision repair and transcriptional regulation: TFIIH and beyond. *Annu Rev Biochem* 85: 265–290
- Davies H, Bignell GR, Cox C, Stephens P, Edkins S, Clegg S, Teague J, Woffendin H, Garnett MJ, Bottomley W et al (2002) Mutations of the BRAF gene in human cancer. *Nature* 417: 949–954
- Eggermont AM, Spatz A, Robert C (2014) Cutaneous melanoma. *Lancet* 383: 816–827
- Eick D, Geyer M (2013) The RNA Polymerase II Carboxy-Terminal Domain (CTD) code. *Chem Rev* 113: 8456–8490
- Eliades P, Abraham BJ, Ji Z, Miller DM, Christensen CL, Kwiatkowski N, Kumar R, Njauw CN, Taylor M, Miao B et al (2018) High MITF expression is associated with super-enhancers and suppressed by CDK7 inhibition in melanoma. *J Invest Dermatol* 138: 1582–1590
- Ennen M, Keime C, Gambi G, Kiény A, Coassolo S, Thibault-Carpentier C, Margerin-Schaller F, Davidson G, Vagne C, Lipsker D et al (2017) MITF-high and MITF-low cells and a novel subpopulation expressing genes of both cell states contribute to intra- and intertumoral heterogeneity of primary melanoma. *Clin Cancer Res* 23: 7097–7107
- Fisher RP (2019) Cdk7: a kinase at the core of transcription and in the crosshairs of cancer drug discovery. *Transcription* 10: 47–56
- Fontanals-Cirera B, Hasson D, Vardabasso C, Di Micco R, Agrawal P, Chowdhury A, Gantz M, de Pablos-Aragoneses A, Morgenstern A, Wu P et al (2017) Harnessing BET inhibitor sensitivity reveals AMIGO2 as a melanoma survival gene. *Mol Cell* 68: 731–744.e9
- Haq R, Shoaq J, Andreu-Perez P, Yokoyama S, Edelman H, Rowe GC, Frederick DT, Hurley AD, Nellore A, Kung AL et al (2013) Oncogenic BRAF regulates oxidative metabolism via PGC1alpha and MITF. *Cancer Cell* 23: 302–315
- Hnisz D, Abraham BJ, Lee TI, Lau A, Saint-Andre V, Sigova AA, Hoke HA, Young RA (2013) Super-enhancers in the control of cell identity and disease. *Cell* 155: 934–947
- Hodis E, Watson I, Kryukov G, Arold S, Imielinski M, Theurillat J-P, Nickerson E, Auclair D, Li L, Place C et al (2012) A landscape of driver mutations in melanoma. *Cell* 150: 251–263
- Hoek KS, Eichhoff OM, Schlegel NC, Dobbeling U, Kobert N, Schaerer L, Hemmi S, Dummer R (2008) *In vivo* switching of human melanoma cells between proliferative and invasive states. *Cancer Res* 68: 650–656
- Kemper K, de Goeje PL, Peeper DS, van Amerongen R (2014) Phenotype switching: tumor cell plasticity as a resistance mechanism and target for therapy. *Cancer Res* 74: 5937–5941
- Khaled M, Levy C, Fisher DE (2010) Control of melanocyte differentiation by a MITF-PDE4D3 homeostatic circuit. *Genes Dev* 24: 2276–2281
- Klein RM, Bernstein D, Higgins SP, Higgins CE, Higgins PJ (2012) SERPINE1 expression discriminates site-specific metastasis in human melanoma. *Exp Dermatol* 21: 551–554
- Kwiatkowski N, Zhang T, Rahl PB, Abraham BJ, Reddy J, Ficarro SB, Dastur A, Amzallag A, Ramaswamy S, Tesar B et al (2014) Targeting transcription regulation in cancer with a covalent CDK7 inhibitor. *Nature* 511: 616–620
- Laurette P, Coassolo S, Davidson G, Michel I, Gambi G, Yao W, Sohler P, Li M, Mengus G, Larue L et al (2019) Chromatin remodellers Brg1 and Bptf are required for normal gene expression and progression of oncogenic Braf-driven mouse melanoma. *Cell Death Differ* 27: 29–43
- Laurette P, Strub T, Koludrovic D, Keime C, Le Gras S, Seberg H, Van Otterloo E, Imrichova H, Siddaway R, Aerts S et al (2015) Transcription factor MITF and remodeller BRG1 define chromatin organisation at regulatory elements in melanoma cells. *Elife* 4: e06857
- Louphrasitthiphol P, Siddaway R, Loffreda A, Pogenberg V, Friedrichsen H, Schepsky A, Zeng Z, Lu M, Strub T, Freter R et al (2020) Tuning transcription factor availability through acetylation-mediated genomic redistribution. *Mol Cell* 79: 472–487.e10
- Love MI, Huber W, Anders S (2014) Moderated estimation of fold change and dispersion for RNA-seq data with DESeq2. *Genome Biol* 15: 550
- Loven J, Hoke HA, Lin CY, Lau A, Orlando DA, Vakoc CR, Bradner JE, Lee TI, Young RA (2013) Selective inhibition of tumor oncogenes by disruption of super-enhancers. *Cell* 153: 320–334
- Menzies AM, Long GV (2014) Systemic treatment for BRAF-mutant melanoma: where do we go next? *Lancet Oncol* 15: e371–e381
- Minnoye L, Taskiran II, Mauduit D, Fazio M, Van Aerschoot L, Hulselmans G, Christiaens V, Makhzami S, Seltenhammer M, Karras P et al (2020) Cross-species analysis of enhancer logic using deep learning. *Genome Res* 30: 1815–1834
- Olsson A, Venkatasubramanian M, Chaudhri VK, Aronow BJ, Salomonis N, Singh H, Grimes HL (2016) Single-cell analysis of mixed-lineage states leading to a binary cell fate choice. *Nature* 537: 698–702
- Rambow F, Marine JC, Goding CR (2019) Melanoma plasticity and phenotypic diversity: therapeutic barriers and opportunities. *Genes Dev* 33: 1295–1318
- Rambow F, Rogiers A, Marin-Bejar O, Aibar S, Femel J, Dewaele M, Karras P, Brown D, Chang YH, Debiec-Rychter M et al (2018) Toward minimal residual disease-directed therapy in melanoma. *Cell* 174: 843–855.e19

- Riesenberg S, Groetchen A, Siddaway R, Bald T, Reinhardt J, Smorra D, Kohlmeier J, Renn M, Phung B, Aymans P *et al* (2015) MITF and c-Jun antagonism interconnects melanoma dedifferentiation with pro-inflammatory cytokine responsiveness and myeloid cell recruitment. *Nat Commun* 6: 8755
- Robey RW, Pluchino KM, Hall MD, Fojo AT, Bates SE, Gottesman MM (2018) Revisiting the role of ABC transporters in multidrug-resistant cancer. *Nat Rev Cancer* 18: 452–464
- Seoane M, Buhs S, Iglesias P, Strauss J, Puller A-C, Müller J, Gerull H, Feldhaus S, Alawi M, Brandner JM *et al* (2019) Lineage-specific control of TFIIH by MITF determines transcriptional homeostasis and DNA repair. *Oncogene* 38: 3616–3635
- Smith MP, Brunton H, Rowling EJ, Ferguson J, Arozarena I, Miskolczi Z, Lee JL, Girotti MR, Marais R, Levesque MP *et al* (2016) Inhibiting drivers of non-mutational drug tolerance is a salvage strategy for targeted melanoma therapy. *Cancer Cell* 29: 270–284
- Son J, Kim M, Jou I, Park KC, Kang HY (2014) IFN- γ inhibits basal and α -MSH-induced melanogenesis. *Pigment Cell Melanoma Res* 27: 201–208
- Sun Z, Yan B (2020) Multiple roles and regulatory mechanisms of the transcription factor GATA6 in human cancers. *Clin Genet* 97: 64–72
- Verfaillie A, Imrichova H, Atak ZK, Dewaele M, Rambow F, Hulselmans G, Christiaens V, Svetlichnyy D, Luciani F, Van den Mooter L *et al* (2015) Decoding the regulatory landscape of melanoma reveals TEADS as regulators of the invasive cell state. *Nat Commun* 6: 6683
- Villicana C, Cruz G, Zurita M (2014) The basal transcription machinery as a target for cancer therapy. *Cancer Cell Int* 14: 18
- Whyte WA, Orlando DA, Hnisz D, Abraham BJ, Lin CY, Kagey MH, Rahl PB, Lee TI, Young RA (2013) Master transcription factors and mediator establish super-enhancers at key cell identity genes. *Cell* 153: 307–319
- Widmer DS, Cheng PF, Eichhoff OM, Belloni BC, Zipser MC, Schlegel NC, Javelaud D, Mauviel A, Dummer R, Hoek KS (2012) Systematic classification of melanoma cells by phenotype-specific gene expression mapping. *Pigment Cell Melanoma Res* 25: 343–353
- Wouters J, Kalender-Atak Z, Minnoye L, Spanier KI, De Waegeneer M, Bravo González-Blas C, Mauduit D, Davie K, Hulselmans G, Najem A *et al* (2020) Robust gene expression programs underlie recurrent cell states and phenotype switching in melanoma. *Nat Cell Biol* 22: 986–998
- Xu L, Shen SS, Hoshida Y, Subramanian A, Ross K, Brunet JP, Wagner SN, Ramaswamy S, Mesirov JP, Hynes RO (2008) Gene expression changes in an animal melanoma model correlate with aggressiveness of human melanoma metastases. *Mol Cancer Res* 6: 760–769
- Zhou Y, Zhou B, Pache L, Chang M, Khodabakhshi AH, Tanaseichuk O, Benner C, Chanda SK (2019) Metascape provides a biologist-oriented resource for the analysis of systems-level datasets. *Nat Commun* 10: 1523